Liquid Crystals

ISSN: (Print) (Online) Journal homepage: https://www.tandfonline.com/loi/tlct20

Suppressed twist in droplets of cholesteric rod-like virus as identified by single particle imaging

Y. Jia, E. Stiakakis & M. P. Lettinga

To cite this article: Y. Jia, E. Stiakakis & M. P. Lettinga (2021) Suppressed twist in droplets of cholesteric rod-like virus as identified by single particle imaging, Liquid Crystals, 48:5, 746-755, DOI: 10.1080/02678292.2020.1817584

To link to this article: https://doi.org/10.1080/02678292.2020.1817584

LIQUID CRYSTALS
2021, VOL. 48, NO. 5, 746–755
https://doi.org/10.1080/02678292.2020.1817584

Taylor & Francis
Taylor & Francis Group

Suppressed twist in droplets of cholesteric rod-like virus as identified by single particle imaging

Y. Jia[a], E. Stiakakis[a] and M. P. Lettinga[a,b]

[a]IBI-4, Forschungszentrum Jülich, Germany; [b]Laboratory for Soft Matter and Biophysics, KU Leuven, Leuven, Belgium

ABSTRACT

The director field configuration of a colloidal chiral nematic liquid crystal confined in droplets is studied in this work. We employ microfluidics to produce monodisperse droplets containing nematic dispersions of *fd* virus surrounded by a carrier oil phase, while we vary the size of the droplet as well as the concentration of the virus. The resulting director fields within the droplets are studied at the single-molecule level, using confocal microscopy. The 3-D structures are linked to polarisation microscopy observations of bright rings, which can be attributed to a cholesteric twist of the director field. We identify boundaries of concentration and size where one and two rings are observed, suggesting suppression of the cholesteric twist by confinement. Single particle confocal observations confirm that indeed the twist in the director field underlies the ring formation, but they also show that the twist is non-monotonous throughout the droplet and much smaller than observed in bulk.

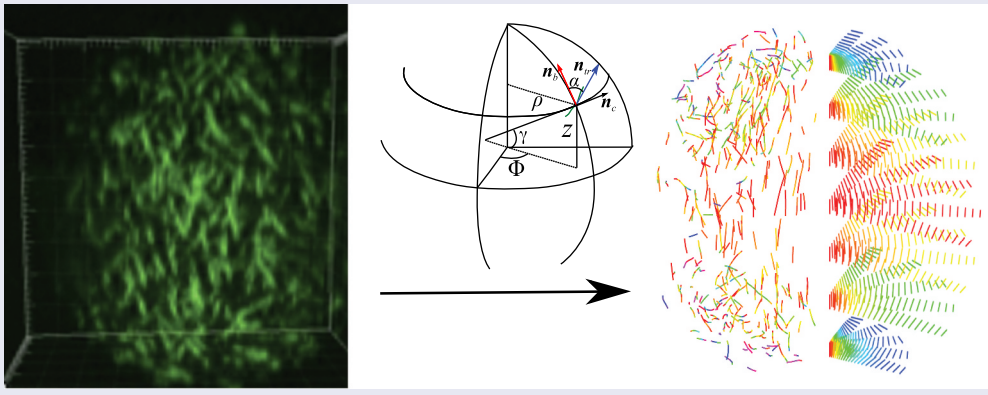

ARTICLE HISTORY
Received 2 June 2020
Accepted 25 August 2020

KEYWORDS
Lyotropic; confinement; confocal microscopy; cholesteric; director field

1. Introduction

When a droplet is formed from a nematic phase, either by phase separation or by fabrication, then the shape of this droplet and the director field are set by the competition between the elastic properties of the nematic liquid crystalline phase, the interfacial tension and the anchoring conditions of the mesogens that constitute the nematic phase [1,2]. Dispersions of colloidal rods often form droplets with a spindle-like shape during phase separation, the so-called tactoids, contrary to thermo-tropic liquid crystals that form spherical droplets [1,3–12]. This is due to the fact that rods tend to align parallel to any wall, thus increasing the freely available volume [13]. The earliest observations of such droplets date back to the pioneering work of Zocher et al. on inorganic colloidal rods [14] and Bernal et al. on colloidal rod-like viruses [15]. The shape and internal structure can be predicted by minimising the total free energy of the three contributions mentioned above [1,2]. This generally yields a transition from a homogeneous to a bipolar configuration as the tactoids grow and the aspect ratio of the tactoids decreases. For the homogeneous configuration, all rods have the same orientation at the expense of the preferred planar anchoring, as exemplified by the orientation of the rods in the schematic drawing in Figure 1(a). In a bipolar configuration, rods are always aligned with the wall at the cost of two surface defects at both poles where there is a splay as shown in Figure 1(b). In experiments on tactoids, the shape and director field of

CONTACT M. P. Lettinga p.lettinga@fz-juelich.de
Supplemental data for this article can be accessed here.

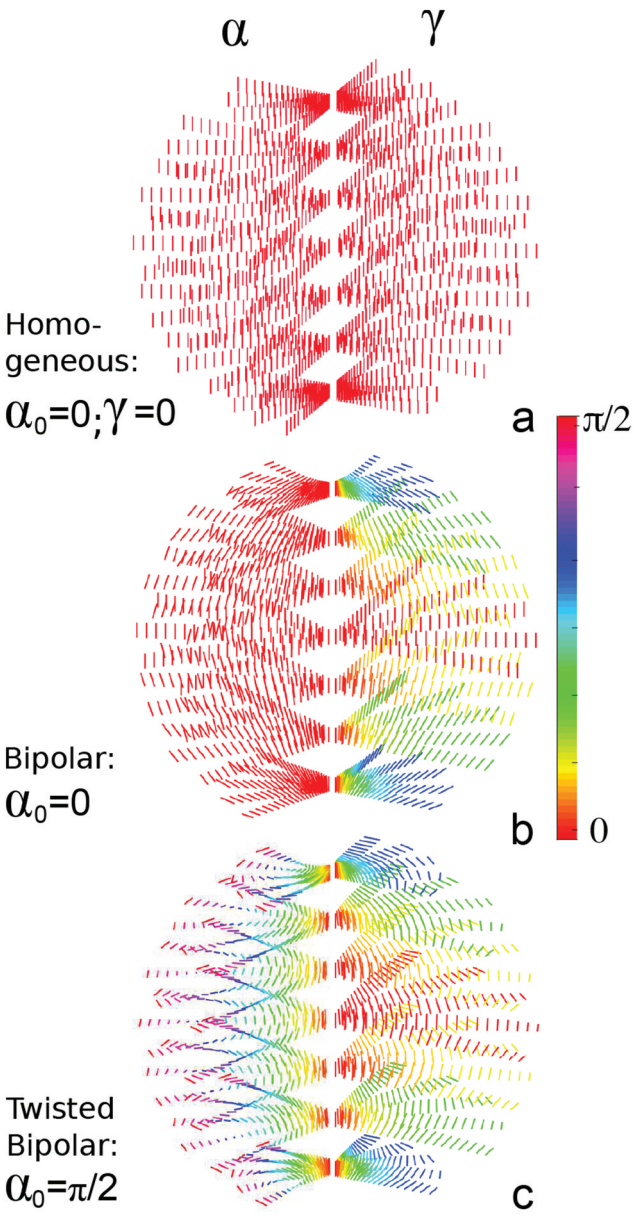

Figure 1. (Colour online) Cuts out of schematic droplets with different director fields as indicated by the orientation of the rods: homogeneous (a); bipolar (b); a twisted bipolar (c). The colour coding is according to the local α (right) and γ (left) in radians, as explained later in Figure 3 and Equations (2)-(3).

the droplet per definition depend on the instant in time during the phase separation at which the tactoids are observed [10,11,16]. Therefore, research so far mostly focused on the relation between shape and size of the droplets. In a recent experiment, however, a transition from a homogeneous to a bipolar director field indeed has been observed for a system of Carbon nanotubes [5,16] and amyloids [10,11]. In the latter system, it was shown how this transition is influenced by the length of the rods.

More complex configurations are found when considering chiral nematics, or cholesteric LCs, which display a twist of the director field due to the intrinsic chirality of the mesogens, characterised by the pitch P of the twist. The question is how the twist can be accommodated in this confinement, given the boundary conditions. Theoretically predicted configurations of the director field for parallel (or tangential) anchored chiral nematic droplets indeed show far more complex configurations than those found for nematic droplets [17–21]. For thermotropic [9,22] and polymeric chiral nematic droplets [23,24] the most prominent structure is the twisted bipolar director field, which is characterised by a constant twist of the director in passing from the middle of the bipolar axis connecting the boojums to the equator at the droplet surfaces as shown in Figure 1(c).

The transition from an untwisted bipolar to a twisted bipolar can, however, also be intrinsically caused by the interplay between confinement and the elasticities that are connected to achiral nematics [21,25–28]. Williams showed how this parity-breaking transition depends on the relation between the splay, twist and bend elastic constants, respectively K_{11}, K_{22} and K_{33} [21]. He concludes that the twisted structure has less splay at the boojums as compared to the untwisted director field, at the cost of twist and bending. A recent study showed that a liquid crystal of achiral rod-like particles forms a macroscopic chiral structure in the confinement of a tactoid, similar to those observed for chiral nematic droplets [27]. In this case, the induced chirality was due to the replacement of the energetically costly splay packing with a less costly twisted packing. Similar observations have been made when packing such a system in a dispersed droplet [28].

Up to recently, no clear evidence of a twisted bipolar was found in tactoids of chiral nematic colloidal rods, such as the well-studied *fd* virus [12,29], despite of the chiral strength K_t that drives the twisting. For the chiral amyloids discussed above, however, an additional cascade of transitions was observed from a bipolar to an uniaxial cholesteric to a radial cholesteric director field, forming, respectively, striped and ring patterns as the size of the droplets increased [10,11]. As the size and therefore the shape cannot be fixed during phase separation, one would ideally like to independently vary the size of the droplets and the equilibrium cholesteric pitch in order to show that the untwist–twist transition depends on these parameters [19,22].

We achieve this goal in this paper by producing aqueous droplets of the chiral rod-like *fd* virus dispersed in oil, similar to Refs. [30,31]. We fix the radius R_0 over a wide range by micro-fluidics, while we fix the equilibrium pitch of cholesteric *fd* dispersions between $P \approx 10$ to 100 μm by varying the concentration. Due to the size of *fd* (contour length of 880 *nm*, persistence length of 2.2

μm, a diameter of 6.6 nm), we can observe the orientation of the particles when labelling them with a fluorescent dye and using confocal microscopy. Hence, we have access to the local director field in three dimensions when tracer amounts of the labelled rods are dispersed in the background of unlabelled rods. This single particle approach has been successfully used to determine the pitch of the cholesteric phase [32] and the director structure in 2-D systems [33–36]. Compared to polarisation microscopy, it has the great advantage that any ambiguity in the interpretation of polarisation images is removed, such as the assumption of a linear twist when going from the symmetry axis to the surfaces [28].

We will start, however, by using polarisation microscopy to construct a diagram of states, indicating transitions between zero, one and two full rings as a function of droplet size and concentrations. We identify these transitions with one and two full rotations of the director field, respectively. We then determine in 3-D the director field configuration by single particle imaging with confocal microscopy, which yields the local orientation in the director field. Contrary to expectations, we will show that confinement suppresses the chiral twist of the *fd* dispersion and that the twist is not constant throughout the droplet.

2. Experimental

The *fd* virus was prepared according to a standard biological protocol using XL1-Blue strain of *E. coli* as the host bacteria [37]. The *fd* virus is dispersed in a TrisHCL buffer (20 mM) with pH 8.0. The concentration of the final virus dispersion is determined spectroscopically using NANODROP (Thermo Fisher Scientific Inc.). Using a confocal microscope, we found a cholesteric pitch of $P = 22\,\mu$m at a concentration of 60 mg/ml and an ionic strength of I = 10 mM. This agrees with the cholesteric pitch as measured for this *fd* concentration and ionic strength as determined by Dogic *et al* [38]. A separate batch of *fd* virus was labelled with Alexa Fluor® 488 (Alexa Fluor® 488 5-TFP, MW of 884.91 mg/mol, Intitrogen™) for single-molecule observations. The fluorescently labelled rods are mixed at a small volume fraction (1–2%) with unlabelled rods, to act as tracers which reveal the director field.

The monodisperse aqueous droplets were generated by dispersing the *fd* virus dispersion into the Pico-Surf™ 1, 2% in FC-40™(Sphere Fluidics Limited), via a pressure-driven Dolomite Microfluidic device (The Dolomite Centre Ltd.). The emulsification took place in a hydrophobic Dolomite Droplet Junction chip with 100 μm etch depth. The generated droplets were collected in flat capillaries (Vitrocom) for observation under the microscope. Patterns formed over two hours to a day, depending on the concentration.

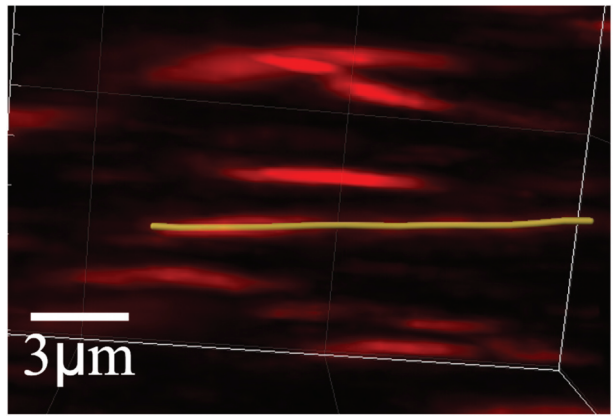

Figure 2. (Colour online) A fitted trace after manually selecting the trace with the help of auto-depth function of IMARIS, with the raw data in the background.

Polarisation microscopy images of the droplets were obtained on a Zeiss Axioplan 2 with Plan-Neofluar objective, 40x, NA = 1.3. The single molecule experiments were performed on the Zeiss LSM 510, equipped with a LCI Plan-Neofluar Gly./W, 63x, NA = 1.3 objective and a single-pinhole confocal unit. We used relatively long exposures resulting in frame rate of 1.93 frames per second. This guarantees a good contrast and, in addition, the long exposure time allows rods to diffuse over relative long distances. Thus, long traces are obtained that mimic the director field as the diffusing rods follow the director field. The microscope was also equipped with a transmission unit so that polarisation images could be obtained.

In the image analysis, we first identified the full 3-D coordinates of the traces which we imaged in the x-y-z scans. To this end, the microscope images were analysed with IMARIS 5.5 (Bitplane AG). Its algorithm is based on the local intensity contrast to the objects of interest. Under the surpass view of IMARIS, the objects are processed as point-like structures. Automatic calculations of the depth of the individual points in the plane of the screen are done by the software, after manually indicating the points at a trace on the screen. The chain of points that is thus generated is used as an input for the final fit of the trace, where an automatic centring is performed. In this way, the positional information in the Cartesian coordinate system was obtained. In Figure 2 we present an example of a fitted trace with the background of raw data.

3. Analysis of director field

3-D traces are transformed into spatial resolved orientational information of the director field throughout the

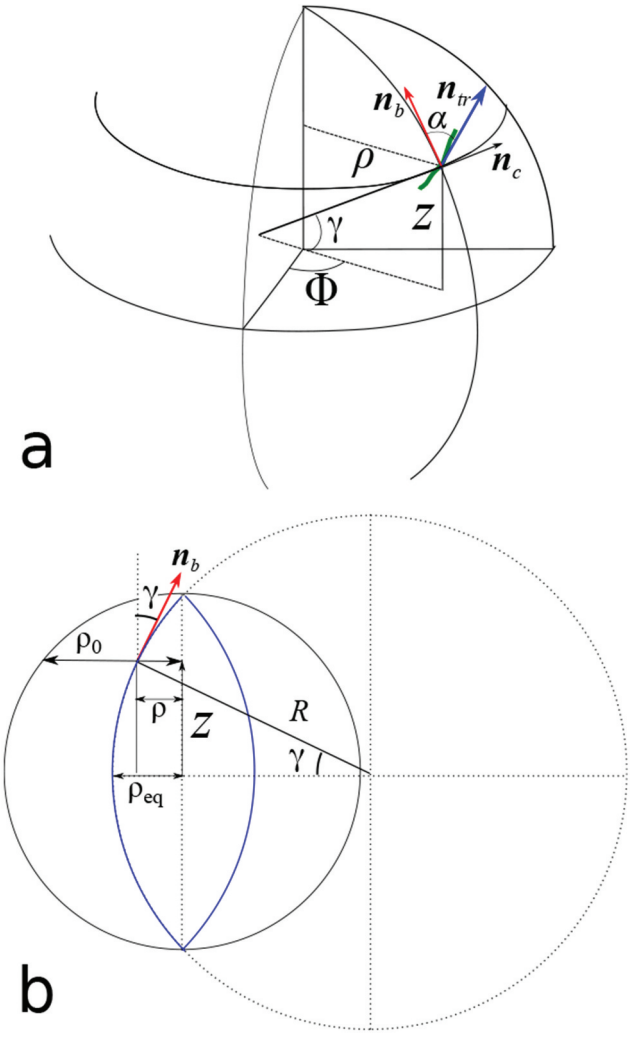

Figure 3. (Colour online) (a) Coordinates for a local trajectory (green line) in a twisted bipolar director field. Figure (b) is used to define the angle γ of $\mathbf{n}_b$ with the symmetry axis.

full droplet by employing the coordinate system as defined by Xu et al. [22]. In this coordinate system, $\mathbf{n}_b$ represents a bipolar director field, where directors lie in the meridional plane and $\mathbf{n}_c$ represents a concentric field, where directors lie in circles parallel to the equatorial plane and concentric with the droplet axis, as shown in Figure 3(a). Due to the cylindrical symmetry of the director field, the location for which the director field is calculated is given in cylindrical coordinates ρ, Φ, Z. The twist is now described by the twisted bipolar director field $\mathbf{n}_{tr}$ according to

$$\mathbf{n}_{tr} = \mathbf{n}_b \cos(\alpha) + \mathbf{n}_c \sin(\alpha), \tag{1}$$

where α is the angle between $\mathbf{n}_{tr}$ and $\mathbf{n}_b$. It is assumed in Ref [22]. that α varies linearly with the distance ρ from the symmetry axis, so that $\alpha = \alpha_0\rho/\rho_0$, where ρ_0 is the maximum radius of the $\rho - \Phi$ cross section at Z, and α_0 is the maximum twist angle. The tilt of $\mathbf{n}_b$ from the symmetry axis is given in our representation by γ, which can be calculated from the tangent of a circle of radius R at the same cross section, as indicated in Figure 3(b). This approach has the advantage that it decouples the effect of wall anchoring, which causes the tilt γ, from the chiral twist, given by α. This is exemplified in Figure 1 by the colour coding: for a normal bipolar distribution α is constant while γ depends on the location in the droplet. For a twisted bipolar director field, γ remains unchanged, while α depends on ρ. In the analysis, we first determine the local tangent of the trace $\mathbf{n}_{tr}$ and calculate α throughout the trace using

$$\alpha = \arccos(\mathbf{n}_{tr} \cdot \mathbf{n}_c), \tag{2}$$

where $\mathbf{n}_c$ is known from the Φ at that location. If indeed $\mathbf{n}_{tr}$ is in a plane with $\mathbf{n}_b$ and $\mathbf{n}_c$, as postulated by Xu et al., then γ can be calculated by

$$\gamma_{tr} = \arccos(z_{tr}/\cos(\alpha)), \tag{3}$$

where z_{tr} is the z-component of $\mathbf{n}_{tr}$ and the subscript is used to indicate the way γ is obtained. When the assumption of Xu et al holds, then γ should namely comply with the γ_p that can be calculated from the position in the droplet, which is given by

$$\gamma_p = 2\arctan\left(\frac{\rho}{Z}\left(\frac{1}{\sqrt{1-Z^2}}\right) - 1\right). \tag{4}$$

4. Results

4.1. Polarisation microscopy

The observed polarisation patterns can be characterised by two classes: a baseball-shaped (Figure 4(c)) and a cross-shaped structure (Figure 4(f-j)), both displaying a superimposed ring structure. The baseball-shaped structure can be changed into a cross-shaped by rotation of the microscope sample stage between crossed polarisers. This is shown subsequently in Figure 4(a-e). In

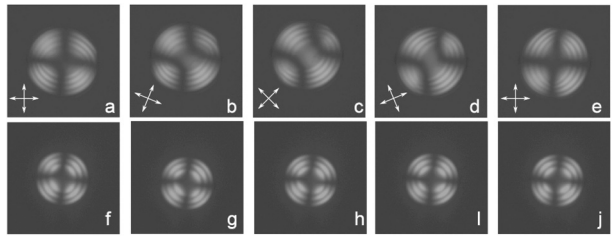

Figure 4. Change in polarisation patterns of droplets by rotating the droplet with respect to the crossed- polarisers ($[fd] = 60\ mg/ml$). The 'baseball' pattern changes (a)-(e), while the 'cross' pattern (f)-(j) does not.Field of view: $500 \times 500\ \mu m$.

contrast, in the other example presented in Figure 4(f-j) the cross-shaped pattern hardly changes during the rotation, while the central part of the droplet remains dark. Both types of pattern are different representations of the same configuration of the director field, owing to the tilting of the symmetry axis of the director field with respect to the glass wall. These kind of ring structures or superposition of ring structures with baseball-shaped and cross-shaped structures have been observed and discussed in literature and are typical for a confined cholesteric phase [9–11,22–24].

We observe that the number of rings depends on the size of the droplet and the concentration of the *fd* virus, irrespective of the underlying pattern. In Figure 5 we plot the areas in a concentration – droplet size diagram where single ring (blue) and two ring (red) structures are observed. The lines indicate a linear fit with a slope of $\approx 0.80 \frac{\mu m}{mg/ml}$. The relation between the concentration and the size of the droplet where the transitions are observed suggests that the ring formation is due to the cholesteric twist which is known to be present in the bulk phase of *fd*. In section 4.2 on the single particle imaging, we give direct experimental evidence that indeed the director field is twisted, although there we are limited to smaller droplets.

Assuming that the formation of the first ring corresponds with the pitch of the cholesteric phase, we can make a comparison with the pitch that is observed in bulk. Therefore, we also plot in Figure 5 the relation between the pitch in bulk P and the concentration $[fd]$ for a comparable ionic strength taken from Ref [38].

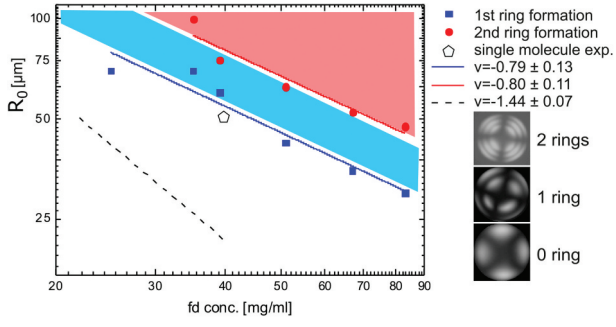

Figure 5. (Colour online) The diagram of states of the polarisation patterns of chiral nematic *fd* virus at varying concentration and confined in droplets of varying radiues R_0: in the red area droplets have two rings; in the blue area they have one ring; below that they have no rings. The states of the mentioned classes are shown on the right. With increasing droplet size: first observed single ring (blue squares); first observed two rings (red dots). The linear fits of these points give a slope v. The black dashed line indicates the predicted transition to the first ring, given the known cholesteric pitch in the bulk phase. The open symbol indicates the droplet for which we present the single particle experiment.

Clearly, the transition is expected to take place much earlier, that is at lower concentrations and for smaller droplets. Also the relation between the pitch and the concentration is different as in bulk the relation $P \propto [fd]^{v}$, with $v = 1.44$, is found. Extrapolating the two lines of the confined pitch and bulk pitch one would expect them to meet when droplets are hundreds of micrometres in diameter. This suggests that the twist is suppressed by the confinement of the droplet.

We did a careful search for multi-ring droplets that show the so-called Frank-Pryce structure. The image depicted Figure 6 displays a collection of droplets that partly merged. For some droplets, one can observe the tendency to form a line defect, as indicated by the red arrows, pointing to regions where the ring structure is broken. For equal sized droplets this is not always observed and it seems therefore that for multiple rings the droplets are in a metastable state. The green arrows point to droplets where clearly no rings form at the core of the droplet. This again suggests that the twist is suppressed. Single particle imaging, as presented in the next section, is needed to gain full insight in this phenomenon.

4.2. Single particle imaging

The use of tracer amounts of the labelled rods dispersed in the background of unlabelled rods allows for an unambiguous characterisation of the director structure in the droplet. We perform such an analysis for the point indicated in the diagram of states displayed in Figure 5, sp fpr droplets with a radius of $R_0 = 50\ \mu m$. A 3-D reconstruction of the traces produced by single

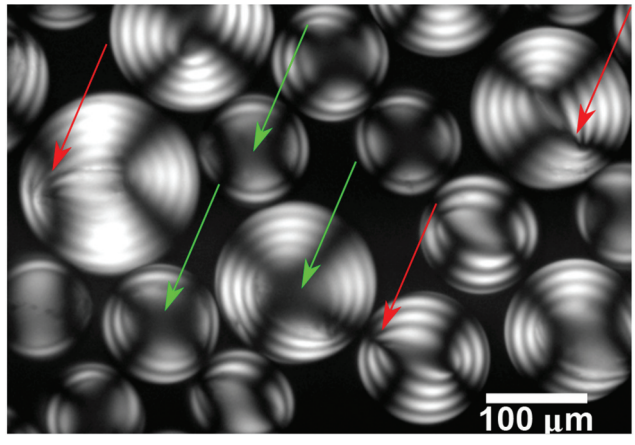

Figure 6. (Colour online) Typical snap shots of highly concentrated *fd* virus droplets ($[fd] = 86\ mg/ml$) of different size. Red arrows indicate regions where the director structrure tends to form a defect line; green arrows indicated the relatively unstructured cores of the droplets.

labelled *fd* particles as obtained by confocal microscopy is presented in Figure 7(a,b). In this example, the droplet is shown both from the x-z and x-y perspective. In the SI† we show a movie of the scan through the droplet. Projections of the same droplet are shown in Figure 7(a) with the symmetry axis of the director field pointing up and in Figure 7(b) with the director field coming out of the plane. From the latter perspective, the traces form part of a circle around the middle of the axis, while traces in the middle of the droplet show up as point-like objects, as they are a projection of the traces on the x-y plane. For the traces further away from the middle axis, their projections on the x-y plane are longer. This is a common feature of all observed droplets. Figure 7(c) displays an overlay of a polarisation pattern and fluorescent traces taken at the equator of the droplet. The fluorescent traces as well as the polarisation pattern suggest a somewhat tilted symmetry axis that comes out of the plane.

In order to perform a full 3-D analysis of the data we first identified the symmetry axis of the director field, by centring the droplet and rotating the coordinates. The rotation should be performed in a way such that a symmetry-axis can be identified for which the distribution of the traces remains unchanged under rotation around this axis. To test if this criterion is met, projections of the rotated traces on the new rotated x-y plane for a centred and rotated dropletare plotted in Figure 8. The colour coding in Figure 8(a) represents the local azimuth angle φ of the trace, which corresponds with the $\mathbf{n}_c$ component of the local tangent of the trace IPGM_A_1816359. By performing a random rotation $\Delta\Phi$ on the traces around the chosen symmetry axis and recalculating the local φ, indeed an identical distribution of colours is obtained. Moreover, the φ-coded colours of the traces depend only on the Φ-component of their location, as defined in Fig.3. This means that the rods always display parallel surface anchoring and that this surface-induced alignment propagates into the droplet. Similarly one can use a colour coding which depends on the twist angle α, see Equation (2). The α colour coding of the projected traces is rotation symmetric around the chosen symmetry axis, while the colour changes from the origin to the boundary. Thus α depends on the distance to the symmetry axis ρ and is independent of Φ as expected for a twisted bipolar director field.

Finally, we confirm in Figure 9(a) that the director field also has mirror symmetry in the equatorial plane by looking at the colour coding of the absolute value of the tilt angle γ. The traces clearly show that the director field is *bipolar*, with two dislocations at the top and the bottom. Moreover, the colour coding indeed displays the mirror symmetry as expected for a bipolar director field. The symmetry is further tested by plotting γ versus ρ, comparing curves at opposite Z cross sections, see Figure 9(b). As γ is rotation symmetric around the z-axis, just as α, we performed an azimuthal average over Φ to obtain these data. Curves for Z and $-Z$ overlay both for γ_{tr} and γ_p. Also the correspondence between the differently calculated values of γ is reasonable. Only the comparison with the calculated γ is not satisfactory for the larger Z-values, probably due to a slight deformation of the droplet caused by gravity.

So far we have merely confirmed with the single particle imaging that the confined director field of the cholesteric *fd* virus is a twisted bipolar field, with the corresponding mirror and rotation symmetries for the tilt angle α and twist angle γ. We now quantify the local twisting structure, by plotting in Figure 10 the averaged α versus ρ, for various distances to the equator Z. Here we exploit the symmetry to azimuthally averaging α over Φ and summing the data of slabs sharing the same absolute Z value within a slab thickness $\Delta Z = 1/7$ of the droplet. α displays a twist from the origin to the lateral boundary for all slabs, as expected for a cholesteric system. There are, however, two important features that do not comply with a freely twisting director field driven by a intrinsic chiral twist K_t of the system. First, the overall increase in α is much smaller than the slopes that can be calculated based on Xu and Crooker's assumption that α varies linearly with ρ,

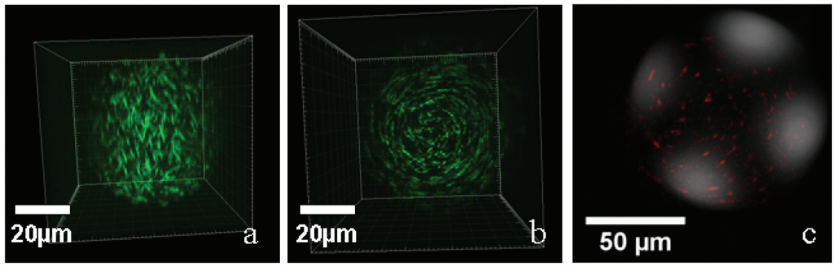

Figure 7. (Colour online) Two perspectives of a three-dimensional fluorescence confocal microscope scan of *fd* virus in a droplet: x-z plane (a) and x-y plane (b). (c) The overlaid image of the polarisation pattern and the confocal scan of a droplet at the equator.

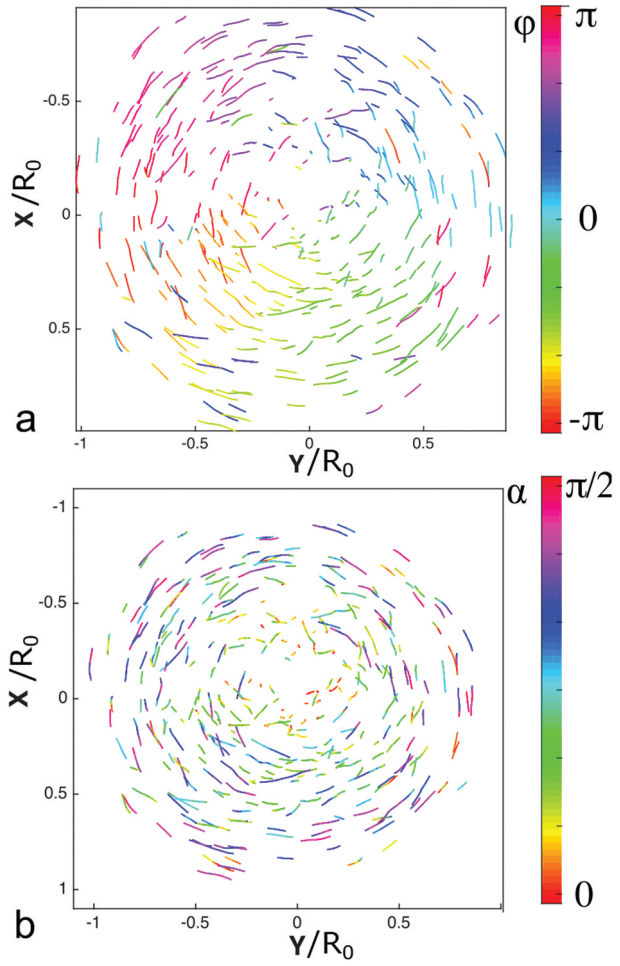

Figure 8. (Colour online) Determination of the symmetry axis in the droplet using projections of the traces of *fd* virus in the rotated x-y plane. The traces are colour coded by their local azimuth angle φ (a) and the twist angle α (b).

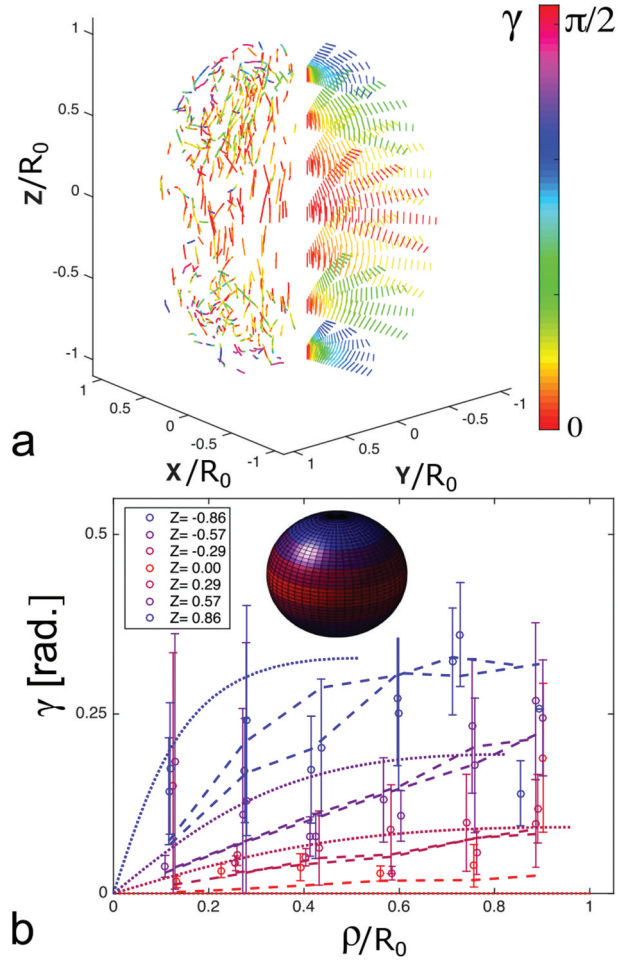

Figure 9. (Colour online) (a) A cut from the director field in an experimental droplet (left) and calculated twisted bipolar with $\alpha_0 = \pi/2$ droplet (right). Traces are colour coded by their local angle γ. (b) γ versus the distance to the symmetry axis ρ for various positions Z, as indicated by the colours and the sphere in the inset.

resulting in the dashed lines in Figure 10. Hence, the twist is suppressed. Second, focusing on the lines close to the equator for which we have good statistics, we observe that the slope is not constant. Close to the symmetry axis the slope is small and only for $\rho \rightarrow 1$ the slope approaches the bulk prediction. Hence, we find that the suppression of the twist is mostly localised close to the symmetry axis. This quantifies the observation of a structureless core in the polarisation images, as indicated by the green arrows in Figure 6. Note also that the end value α at the equator of $\alpha \approx 90^\circ$ is consistent with the fact that the studied sample corresponds with a point in the diagram of states close to the line where one ring is observed, as can be seen in Figure 5.

5. Discussion

There are two ways to explain our observation of a parity breaking twisted bipolar structure for the confined colloidal chiral nematic system. It can be 'twist'-driven, in order to accommodate the intrinsic twist of chiral nematic systems [17,18]; it can be 'splay'-driven as the twisted bipolar has less splay at the boojums compared to the untwisted bipolar director field, at the cost of twist and bending [21,25–28]. The lowest energy state is reached in both cases, but in the first case the system needs to be chiral, while in the second case also achiral nematics will twist. For both mechanisms predictions have been made as to where in the droplet size-pitch diagram the twisted bipolar should be located.

First, we consider the Williams condition for parity breaking to form a twisted bipolar for achiral rods, $K_{11} > K_{22} + 0.431K_{33}$. We know that $K = K_{11} \approx K_{33}$ for the relative flexible *fd* [33]. The Williams condition can thus be rewritten to $0.569K_{11} > K_{22}$. From Ref [38], we know that $K_{22} \approx 1 \times 10^{-7}$ *dyne*, while from Ref [39], we

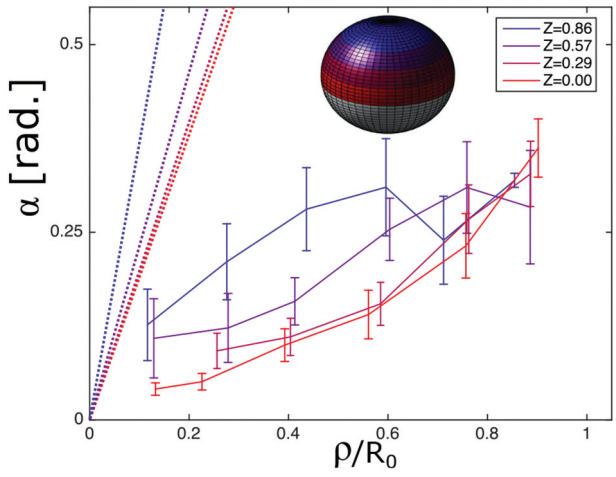

Figure 10. (Colour online) The chiral twist angle angle α versus the distance to the symmetry axis ρ for various positions Z, as indicated by the colours and the sphere in the inset. The dashed lines are the calculated lines assuming that $\alpha = \alpha_0\rho/\rho_0$, where α_0 is set by the pitch in bulk.

know that $K \approx 1 \times 10^{-8}$ *dyne*. One could thus conclude that the formation of the twisted bipolar is 'twist'-driven, as the condition for 'splay'-driven twisted bipolar formation is not fulfilled. The cholesteric twist K_t is needed to yield the twisted structure. This mechanism is not applicable to the earlier observed achiral particles [21,25–28].

On the other hand, more complex 'twist'-driven configurations than the twisted bipolar presented here, have been predicted [17,18] and observed [10,11,22–24,30,31] for chiral nematics. The Frank-Pryce configuration, which has a radial disclination, is found for relatively stronger pitches and has been found for amyloids [10,11], and cellulose nanocrystals [30,31]. A criterion for the formation of such a structure is given by $P \leq 4R/3$, where P is the pitch and R is the radius of the droplet. In principle this criterion has been fulfilled for a major part of the phase diagram, when considering the bulk value for the pitch. For the largest droplets we do observe hints of the formation of this structure, as shown in Figure 6, but certainly no clear Frank-Pryce configurations are found. This complies with one of the important findings of this paper, which is that the pitch in the twisted bipolar droplets is about a factor two bigger as it is in bulk. This means that the director field unwinds as the chiral dispersion is confined in the droplet and the twist is suppressed, for which again indications can be found for the highly chiral amyloids and cellulose nanocrystals[10, 30**?**,31]. Thus, the suppressed pitch should be used to predict transitions to more complex configurations, such as observed in 2D by Gibaud et al [40]. The observation that confinement hugely affects director structure is also reflected in metastability of the director structure, which is apparent from the fact that line droplets with exactly the same size and concentration of *fd* display director fields that co-exist with and without defect lines. In Ref [36]. it was indeed shown that director fields can be stuck in a metastable state due to confinement.

Comparing the behaviour of nematic the *fd* droplets with tactoids that form during phase separation, we can conclude that the high surface tension between oil and water is sufficient to counterbalance the splay driven formation of spindle-shaped droplets [19], even for high concentrations and small droplets. Thus, the oil–water interface acts as a hard wall at which the particles anchor in parallel. The fact that the twist is largely suppressed in the droplets complies with the fact that for *fd* no twist has been observed in tactoids, which is of course also related to the low concentration of rods in the phase coexisting nematic. It can be speculated that the flexibility of the rods also plays an important role. As the bend elasticity is much higher for ridged rods- see recent experiments and simulations on confined *fd* [33]- the state-diagram might shift considerably when using e.g. $fd - Y21M$, which is about 5 times stiffer than the wild type *fd* [20,41].

Finally, we note that the non-monotonous behaviour of the twist means that a constant twist, as it is assumed in the main theoretical approach Refs. [17,18] and in the interpretation of polarisation data [28], is not applicable. Further advances in theory are needed to gain full understanding of these crowding effects. A 3-D fitting routine of the Frank free energy needs to be applied to fit the fractions of the 3-D director field that we presented here, but the structure will look as sketched in Figure 9a, right half.

6. Conclusion

We characterised the director field of a cholesteric *fd* dispersion in droplets surrounded by the oil phase, which were produced using a microfluidic device. Polarisation images already suggested that the cholesteric twist in the director field is suppressed by confinement of the droplets. Single particle imaging, using confocal microscopy, show unambiguously, and independently of the orientation of the droplet, that a twisted bipolar director field is formed. More importantly, with this approach important details on the structure are obtained: the twist is non-monotonous and indeed much suppressed by confinement. This result calls for new theoretical investigations, as in theory twist was thus far assumed to be constant throughout the droplet.

Acknowledgments

Eric Grelet, Jan Dhont, Miha Ravnik, and Alberto Fernandez-Nieves are thanked for fruitful discussions. We thank the group of Prof. R. Merkel (IBI-2) for the use of the confocal microscope.

Disclosure statement

No potential conflict of interest was reported by the author(s).

References

[1] Kaznacheev AV, Bogdanov MM, Taraskin SA. The nature of prolate shape of tactoids in lyotropic inorganic liquid crystals. J Exp Theo Phys. 2002;950 (1):57–63.
[2] Prinsen P, van der Schoot P. Shape and director-field transformation of tactoids. Phys Rev E. 2003;68:021701.
[3] Kaznacheev AV, Bogdanov MM, Sonin AS. The influence of anchoring energy on the prolate shape of tactoids in lyotropic inorganic liquid crystals. J Exp Theo Phys. 2003;970(6):1159–1167.
[4] Candau S, Leroy P, Debeauva. F. Magnetic-field effects in nematic and cholesteric droplets suspended in an isotropic liquid. Mol Crys Liqu Crys. 1973;230 (3–4):283–297.
[5] Puech N, Grelet E, Poulin P, et al. Nematic droplets in aqueous dispersions of carbon nanotubes. Phys Rev E. 2010;820(2):020702(R).
[6] Viamontes J, Oakes PW, Tang JX. Isotropic to nematic liquid crystalline phase transition of f-actin varies from continuous to first order. Phys Rev Lett. 2006;97:118103.
[7] Oakes PW, Viamontes J, Tang JX. Growth of tactoidal droplets during the first-order isotropic to nematic phase transition of f-actin. Phys Rev E. 2007;75:061902.
[8] Castellon E, Zayat M, Levy D. Molecular configuration transitions of a nematic liquid crystal encapsulated in organically modified silicas. PCCP. 2009;110 (29):6234–6241.
[9] Lopez-Leon T, Fernandez-Nieves A. Drops and shells of liquid crystal. Coll Pol Sci. 2011;2890(4):345–359.
[10] Bagnani M, Nystrom G, De Michele C, et al. Amyloid fibrils length controls shape and structure of nematic and cholesteric tactoids. Acs Nano. 2019;130 (1):591–600.
[11] Nystrom G, Arcari M, Mezzenga R. Confinement-induced liquid crystalline transitions in amyloid fibril cholesteric tactoids. Nat Nanotechnol. 2018;130(4):330.
[12] Modlinska A, Alsayed AM, Gibaud T. Condensation and dissolution of nematic droplets in dispersions of colloidal rods with thermo-sensitive depletants. Sci Rep. 2015;5:18432.
[13] Dijkstra M, van Roij R, Evans R. Wetting and capillary nematization of a hard-rod fluid: A simulation study. Phys Rev E. 2001;630(5):051703.
[14] Zocher H. Uber freilwillige strukturbildung in solen. Z Anorg Allg Chem. 1925;147:91–110.
[15] Bernal JD, Fankuchen I. X-ray and crystallographic studies of plant virus preparations i. introduction and preparation of specimens i. modes of aggregation of the virus particles. J Gen Physiology. 1941;250(1):111–146.
[16] Jamali V, Behabtu N, Senyuk B, et al. Experimental realization of crossover in shape and director field of nematic tactoids. Phys Rev E. 2015;910(4):042507.
[17] Bezic J, Zumer S. Structures of the cholesteric liquid-crystal droplets with parallel surface anchoring. Liq Cryst. 1992;110(4):593–619.
[18] Sec D, Porenta T, Ravnik M, et al. Geometrical frustration of chiral ordering in cholesteric droplets. Soft Matter. 2012;80(48):11982–11988.
[19] Prinsen P, van der Schoot P. Parity breaking in nematic tactoids. J Phys-Cond Matt. 2004;160(49):8835–8850.
[20] Barry E, Beller D, Dogic Z. A model liquid crystalline system based on rodlike viruses with variable chirality and persistence length. Soft Matter. 2009;5:2563–2570.
[21] Williams RD. 2 transitions in tangentially anchored nematic droplets. J Phys A. 1986;190(16):3211–3222.
[22] Xu F, Crooker PP. Chiral nematic droplets with parallel surface anchoring. Phys Rev E. 1997;560(6):6853–6860.
[23] Yang DK, Crooker PP. Field-induced textures of polymer-dispersed chiral liquid-crystal microdroplets. Liq Cryst. 1991;90(2):245–251.
[24] Filas RW. Tactoidal shell defects in poly (gamma-benzyl-d-glutamate) liquid-crystals. J De Phys. 1978;390(1):49–55.
[25] Lavrentovich OD, Sergan VV. Parity-breaking phase-transition in tangentially anchored nematic drops. Nuovo Cimento Della Societa Italiana Di Fisica D-Condensed Matter Atomic Mol Chem Phys Fluids Plasmas Biophys. 1990;120(9):1219–1222.
[26] Hough LE, Jung HT, Kruerke D, et al. Helical nanofilament phases. Science. 2009;3250(5939):456–460.
[27] Tortora L, Lavrentovich OD. Chiral symmetry breaking by spatial confinement in tactoidal droplets of lyotropic chromonic liquid crystals. PNAS. 2011;1080 (13):5163–5168.
[28] Jeong J, Davidson ZS, Collings PJ, et al. Chiral symmetry breaking and surface faceting in chromonic liquid crystal droplets with giant elastic anisotropy. PNAS. 2014;1110(5):1742–1747.
[29] Lettinga MP, Kang K, Imhof A, et al. Kinetic pathways of the nematic-isotropic phase transition of rod-like viruses. J Phys Condens Matter. 2005;17:S3609–S3681.
[30] Li YF, Suen JJY, Prince E, et al. Colloidal cholesteric liquid crystal in spherical confinement. Nat Commun. 2016;7:12520.
[31] Li YF, Prince E, Cho SH, et al. Periodic assembly of nanoparticle arrays in disclinations of cholesteric liquid crystals. PNAS. 2017;1140(9):2137–2142.
[32] Tombolato F, Ferrarini A, Grelet E. Chiral nematic phase of suspensions of rodlike viruses: left-handed phase helicity from a right-handed molecular helix. Phys Rev Lett. 2006;960:25.
[33] Dammone OJ, Zacharoudiou I, Dullens RP, et al. Confinement induced splay-to-bend transition of colloidal rods. Phys Rev Lett. 2012;1090(10):108303.
[34] Lewis AH, Garlea I, Alvarado J, et al. Colloidal liquid crystals in rectangular confinement: theory and experiment. Soft Matter. 2014;100(39):7865–7873.
[35] Garlea IC, Mulder P, Alvarado J, et al. Finite particle size drives defect-mediated domain structures in

strongly confined colloidal liquid crystals. Nat Commun. 2016;7:12112.
[36] Garlea IC, Dammone O, Alvarado J, et al. Colloidal liquid crystals confined to synthetic tactoids. Sci Rep. 2019;9:20391.
[37] Sambrook J, Fritsch EF, Maniatis T. Molecular cloning: a laboratory manual. Cold Spring Harbor, New York: Cold Spring Harbor Laboratory Press; 1989.
[38] Dogic Z, Fraden S. Cholesteric phase in virus suspensions. Langmuir. 2000;160(20):7820–7824.
[39] Dogic Z, Zhang J, Lau AWC, et al. Elongation and fluctuations of semiflexible polymers in a nematic solvent. Phys Rev Lett. 2004;920(12):125503.
[40] Gibaud T, Barry E, Zakhary MJ, et al. Reconfigurable self-assembly through chiral control of interfacial tension. Nature. 2012;481:348–351.
[41] Pouget E, Grelet E, Lettinga MP. Dynamics in the smectic phase of stiff viral rods. Phys Rev E. 2011;84:041704.